

Partial-to-Full Registration based on Gradient-SDF for Computer-Assisted Orthopedic Surgery

Tiancheng Li¹, Peter Walker², Danial Hammoud², Liang Zhao³, and Shoudong Huang¹

Abstract—In computer-assisted orthopedic surgery (CAOS), accurate pre-operative to intra-operative bone registration is an essential and critical requirement for providing navigational guidance. This registration process is challenging since the intra-operative 3D points are sparse, only partially overlapped with the pre-operative model, and disturbed by noise and outliers. The commonly used method in current state-of-the-art orthopedic robotic system is bony landmarks based registration, but it is very time-consuming for the surgeons. To address these issues, we propose a novel partial-to-full registration framework based on gradient-SDF for CAOS. The simulation experiments using bone models from publicly available datasets and the phantom experiments performed under both optical tracking and electromagnetic tracking systems demonstrate that the proposed method can provide more accurate results than standard benchmarks and be robust to 90% outliers. Importantly, our method achieves convergence in less than 1 second in real scenarios and mean target registration error values as low as 2.198 mm for the entire bone model. Finally, it only requires random acquisition of points for registration by moving a surgical probe over the bone surface without correspondence with any specific bony landmarks, thus showing significant potential clinical value. The MATLAB code of the framework is available*.

Index Terms—Bone registration, Partial-to-full registration, gradient-SDF, Computer-aided orthopedic surgery

I. INTRODUCTION

OSTEOARTHRITIS constitutes a major musculoskeletal burden for aged people worldwide. The demand for computer-assisted orthopedic surgery (CAOS) for treating osteoarthritis has grown substantially, especially total hip replacements (THR) and total knee arthroplasty (TKA). The bone registration is a fundamental requirement for providing navigational guidance in CAOS [1]. Its main task is to bring the pre-operative computerised tomography (CT) or magnetic resonance imaging (MRI) space and the intra-operative patient space together [3] by solving the transformation matrix between two bone point sets [2], which is necessary for accurate surgical planning and placement of implants. The pre-operative model (full bone point sets) which is typically global and complete, and can be obtained by segmenting the bone from the CT or MRI volume [15]. The intra-operative partial point

set is usually obtained from medical devices such as optical tracking system, endoscopic camera, electromagnetic tracking, CT or X-ray during the procedure [16]–[20].

The most natural and commonly used registration method is to use a surgical tracking probe to verify and acquire multiple bony landmarks intra-operatively corresponding to the pre-operative model [22]. However, it is difficult to accurately recognize and touch the exact landmarks during surgery due to blood and surface tissue interference [21]. Errors in landmark selection can also severely affect the accuracy and robustness of registration. Therefore, the current robotic systems for orthopedic surgery require the surgeon to select as many bony landmarks as possible for registration to increase error tolerance and improve the registration accuracy. For example, the current state-of-the-art orthopedic robotic system, MAKO Robotic Arm Interactive Orthopedic System (Stryker), needs more than 30 landmarks to be accurately touched by the probe as shown in Fig. 1. This approach will lead to an increase in the average surgery time and potential registration error due to the possible invisibility of the landmarks during surgery [22].

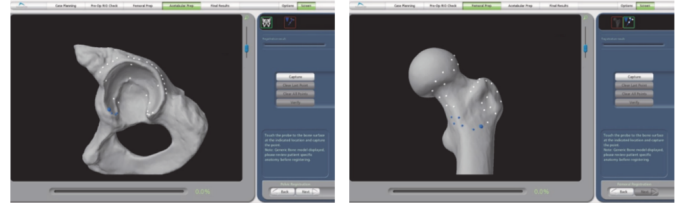


Fig. 1. Registration pattern for pelvis and femur in MAKO [22]. The dots show the bony landmarks to be accurately verified and acquired by the probe for registration.

A better alternative is to randomly acquire points by moving the surgical tracking probe over the bone surface intra-operatively and align with the pre-operative 3D model. However, there are multiple challenges: (i) As only part of the bone can be exposed intra-operatively, the acquired points could only partially overlap with the pre-operative model. The partial anatomy can lead to limited spatial and structural information for the registration; (ii) Intra-operatively acquired points are usually disturbed by noise and outliers. The low-quality point sets can affect the accuracy of the registration. (iii) The intra-operative points are sparse, resulting in minimal structural features and increasing the registration difficulty.

In this paper, we propose a robust and accurate partial-to-full registration approach based on gradient signed distance field (gradient-SDF) [23] to address the above mentioned challenges. The simulation experiments on multi-category

This work was supported by the National Health and Medical Research Council (NHMRC) Ideas Grant, Australia (No. 2029811).

¹Tiancheng Li and Shoudong Huang are with the Robotics Institute, Faculty of Engineering and Information Technology, University of Technology Sydney (UTS), Australia (e-mail: tiancheng.li-1@student.uts.edu.au; shoudong.huang@uts.edu.au).

²Peter Walker and Daniel Hammoud are with the Concord Repatriation General Hospital, New South Wales, Australia.

³Liang Zhao is with the School of Informatics, The University of Edinburgh, United Kingdom (e-mail: liang.zhao@ed.ac.uk).

*<https://github.com/utsTianchengLi/Bone-registration-for-CAOS>

bone structures from publicly available datasets, and real phantom experiments under both optical tracking and electromagnetic tracking systems show the competitiveness of the proposed framework: (i) Gradient-SDF can provide more accurate gradients so that it ensures accurate registration and fast convergence for sparse point clouds without the need for correspondences. (ii) Using M-estimator with Cauchy’s residual function can effectively remove outliers and improve robustness to noise. (iii) Our approach only require random acquisition of points by moving the probe over the bone surface, which can lead to saving of surgical time and cost. (iv) It can be easily integrated clinically, without interrupting the workflow of COAS.

II. RELATED WORK

Traditional registration methods. The Iterative Closest Point (ICP) algorithm [4] is considered a milestone in point cloud registration, which is an iterative algorithm estimating the pose and correspondence simultaneously. However, ICP is prone to converge to local minima and only performs well given an accurate initial guess [5]. Multiple variants of ICP have been proposed, including those using normal information [2], [6], incorporating uncertainty in measurements [33] or finding correspondence [34]. To further improve the robustness and accuracy of the point cloud registration, methods based on probabilistic interpretations have been proposed. For example, Gaussian Mixture Model (GMM) [7] represents two point sets in search of the optimal transformation. Coherent Point Drift (CPD) [8] is also one classic method in this category, where one point set is considered as the centers of the Gaussian mixtures and the other point set is generated by the mixtures. JRMPIC [9] generalises CPD to the case where multiple point sets are registered simultaneously. Motivated by getting the globally optimal solution, Go-ICP [31] adopts a branch and bound technique to search the entire 3D motion space. TEASER [5] reformulates the registration problem using a Truncated Least Squares (TLS) cost and solves it by a general graph-theoretic framework.

Learning-based registration methods. The breakthroughs in deep learning for 3D point clouds (e.g., PointNet [10] and DGCNN [11]) present new prospects for learning point cloud registration directly from data. PointNetLK [12] uses PointNet to learn feature representation, and then align source and target point set features, thereby enabling them to be aligned. However, PointNetLK is mainly proposed for point set pairs with a high ratio of overlapping. To address the challenge of partial overlap, PRNet [13] extends DCP [14] to aligning partially overlapped point clouds by employing a Siamese DGCNN [11] for feature embedding. Nevertheless, these methods that perform well are overwhelmingly based on correspondence and are difficult to ensure generalization when transferred to novel registration tasks [15].

Registration in CAOS. Depending on the data type, point set registration problems in CAOS can be classified into 2D-to-3D registration and 3D-to-3D registration problems [35]. Focusing on our 3D-to-3D rigid point set registration case, the most commonly used method is the landmark-based registration [22]. It is also the current method used by

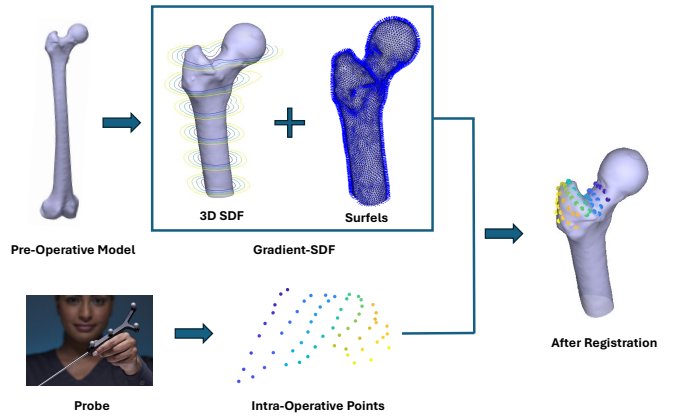


Fig. 2. Our framework: the pre-operative model is represented as gradient-SDF which is a hybrid representation between standard SDF stored in a voxel grid and explicit geometry representation using surfels (surface normal). The intra-operative points are collected by moving the probe over the bone surface.

the MAKO robot. Lots of anatomical landmarks of interest need to be precisely localised in both the pre-operative and intra-operative spaces, which is time consuming and error-prone [3]. Motivated by the use of a small number of sparse measurements probing-based surgical registration, Srivatsan *et al.* [36] propose two variants for sparse point and normal registration (SPNR), namely deterministic (dSPNR) and probabilistic (pSPNR). However, as the name suggests, the methods require surface normal measurements for the intra-operative acquired points. Although the authors suggest that real scenarios can end up with a robotic arm to help obtain the normal vector information, this would also add cost and time. Min *et al.* [21] utilized the tangent vectors extracted from the sparse intra-operative data points and the normal vectors extracted from the pre-operative model points for registration, which also increases the surgeon’s intra-operative workload.

This paper aims to address the above challenges and issues. The main contributions can be summarized as:

- We propose a novel and robust framework based on gradient-SDF for a challenging scenario: registration from a sparse and partial point set to another full model.
- The proposed method does not require correspondence, but only random acquisition of points by moving a probe over the bone surface, thus simplifying the surgeon’s work during intra-operative registration and showing significant potential clinical value.
- Experiments on multi-category sawbones models were carried out in both optical and electromagnetic tracking systems to verify that our framework can obtain accurate registration results in real scenarios with very fast convergence rates.

III. METHODOLOGY

A. Optimisation Problem Formulation

For the standard CAOS, the pre-operative model is obtained from CT scan or MRI. The model is the full 3D point set, and the first step in our algorithm is to represent it as gradient-SDF which is a voxel grid where each voxel contains its Euclidean

distance to the nearest object surface (Fig. 2). Different from the standard SDF, gradient-SDF also pre-calculates and stores the gradients for each voxel using the surface normal property of a surfel [23].

The sparse point cloud p_k ($k \in \{1, \dots, K\}$) is randomly acquired by moving the tracking probe on the bone surface intra-operatively (Fig. 2). The goal is to transform this point cloud to the surface of the model, that is, the zero set level of the gradient-SDF such that $SDF(p) = 0$, where $p \in \mathbb{R}^3$ is a point in the space. Then, the problem is estimating a rigid motion with rotation $\mathbf{R} \in SO(3)$ and the translation $\mathbf{t} \in \mathbb{R}^3$, which minimises the following function:

$$F(X) = \sum_{k=1}^K \|f_k(X)\|^2 = \sum_{k=1}^K \|SDF(\mathbf{R} \cdot p_k + \mathbf{t})\|^2. \quad (1)$$

where $X = (\mathbf{R}, \mathbf{t})$ is the state, and $f_k(X)$ is the closest distance from p_k to the object surface. Applying Gauss-Newton method, for each iteration with initial state $X^{(n)}$, the optimal update ΔX^* can be obtained by

$$\Delta X^* = \arg \min_{\Delta X} \sum_{k=1}^K \|SDF(P_k(X^{(n)} \oplus \Delta X))\|^2, \quad (2)$$

where

$$\begin{aligned} P_k(X) &= \mathbf{R} \cdot p_k + \mathbf{t}, \\ X \oplus \Delta X &= (\exp(\xi^\wedge) \cdot \mathbf{R}, \mathbf{t} + \phi), \end{aligned} \quad (3)$$

and $\Delta X = [\xi, \phi] \in \mathbb{R}^6$ is the update increment. $(\cdot)^\wedge$ is the skew-symmetric operator, and $\exp(\cdot)$ is the matrix exponential map. Then, the state $X^{(n+1)}$ is updated by

$$X^{(n+1)} = X^{(n)} \oplus \Delta X^*. \quad (4)$$

When the algorithm converges, we can obtain the solution of problem (1).

In particular, the Jacobians in the above Gauss-Newton iterations are calculated as

$$J_k(X) = \frac{\partial f_k(X)}{\partial X} = \nabla_{SDF}(P_k(X)) \cdot \frac{\partial P_k(X)}{\partial X}, \quad (5)$$

where $\nabla_{SDF}(\cdot)$ represent the gradient, which is equal to the inwards-pointing surface normal at the closest surface point, and the negative of the outwards-pointing surface normal [23]. And

$$\frac{\partial P_k(X)}{\partial X} = [-(\mathbf{R} \cdot p_k)^\wedge, \mathbf{I}_{3 \times 3}]. \quad (6)$$

Solving the formulated optimisation problem using the above method is computationally efficient since the distance space $SDF(\cdot)$ and the gradient $\nabla_{SDF}(\cdot)$ can be pre-calculated on the pre-operative data. This gradient naturally contains the geometric properties that are not present in the gradients calculated by standard SDF, so the convergence is better and faster.

B. Robust M-estimator against Noise and Outliers

The robustness of the method is crucial since the intra-operative acquired partial points may also be susceptible to noise and outliers due to interference between medical devices. The robust M-estimators (maximum likelihood type

estimators) are originally used to reduce the effect of outliers and to find the maximum likelihood estimate and now have been used in many simultaneous localisation and mapping (SLAM) applications [24]. In this work, we propose to loop over M-estimator with a re-descending influence function to remove the outliers and against the noise. The idea behind it is to design and solve a sequence of intermediate optimization problems $\mathcal{P}_1, \dots, \mathcal{P}_N$ so that (i) the solution of each problem \mathcal{P}_i can be used as the initial guess to obtain the maximum likelihood estimate in the next problem \mathcal{P}_{i+1} , and (ii) the solution of the final problem \mathcal{P}_N is within the basin of attraction of the global minimum of the original least squares problem (1).

Similar to the idea of Graduated Non-Convexity [25], $\{\mathcal{P}_i\}_{i=1}^N$ can be defined as assigning additional weights $w_k^{(i)}$ to all the acquired points p_k such that measurements with large residuals in \mathcal{P}_i will update smaller weights for \mathcal{P}_{i+1} . So the i th intermediate optimization problem \mathcal{P}_i can be formulated as extending the (1) to

$$X_{(i)}^* = \arg \min_X \sum_{k=1}^K w_k^{(i)} \|f_k(X)\|^2. \quad (7)$$

This is similar to the iterated re-weighted least squares (IRLS) problem formulated in M-estimators to reduce the effect of outliers [26]. Large residuals in this problem correspond to the potential outliers or noisy acquired points. As the iterations proceed, the weights assigned to the parts with large residuals become smaller and smaller until they are negligible.

C. Selection of the M-estimator

Instead of the squared residuals, the M-estimators apply another function of the residuals, yielding

$$\min \sum_{k=1}^K \rho(e_k), \quad (8)$$

where $e_k \triangleq \|f_k(X)\|_2$ denotes the ℓ_2 -norm of $f_k(X)$ and $\rho(\cdot)$ is a symmetric positive-definite function with a unique minimum at zero with increments less than squared residuals. In this paper, we use Cauchy's function, since it is more stable against different environment types [38]. For the Cauchy's function we have [26]:

$$\rho(e_k) \triangleq \frac{c^2}{2} \log\left(1 + \left(\frac{e_k}{c}\right)^2\right). \quad (9)$$

Equation (8) can be implemented as an IRLS problem by computing the gradient w.r.t. X and setting it to zero:

$$\sum_{k=1}^K \psi(e_k) \frac{\partial e_k}{\partial X} = 0, \quad (10)$$

where $\psi(x) \triangleq d\rho(x)/dx$ is the influence function and the weight function can be defined as $w(x) \triangleq \psi(x)/x$, then (10) can be re-written as:

$$\sum_{k=1}^K w(e_k) e_k \frac{\partial e_k}{\partial X} = 0. \quad (11)$$

Algorithm 1 Robust registration framework based on gradient-SDF and M-estimator

Input: Full point set \mathbf{P} ; sparse point set: $\{p_k\}_{k=1}^K$.

Output: Optimal transformation X^* .

```

1: Represent  $\mathbf{P}$  as gradient-SDF.
2: Initial transformation  $X^{(0)}$ .
3:  $X_{(0)}^* \leftarrow X^{(0)}$ 
4: loop
5:   repeat
6:     for each  $p_k$  do
7:       Calculate  $e_k^{(i-1)}$  using  $X_{(i-1)}^*$  by (1) and (8)
8:        $w_k^{(i)} = w(e_k^{(i-1)})$  // Cauchy M-estimator
9:     end for
10:    Calculate  $X_{(i)}^*$  by solving the optimization in (7)
    with  $X_{(i-1)}^*$  as initial value
11:     $i \leftarrow i + 1$ 
12:  until  $\|w^{(i)} - w^{(i-1)}\| \leq \varepsilon$  // Converge
13:  if exist  $w_k^{(i)} < \delta$  then
14:    Discard the corresponding  $p_k$  // Outliers
15:     $\{p_k\}_{k=1}^K \leftarrow \{p_k\}_{k=1}^{K^*}$  and continue the loop
16:  else
17:     $X^* = X_{(i)}^*$ 
18:  end if
19: end loop

```

This is the exact system of equations that results from solving the following IRLS problem

$$\min \sum_{k=1}^K w(e_k^{(i-1)}) e_k^2, \quad (12)$$

where the superscript i indicates the iteration number, $e_k^{(i-1)}$ is the residual calculated using the latest estimate, and the weight $w(e_k^{(i-1)})$ need to be re-computed after each iteration for the next estimation. It is noted that (12) is consistent with the underlying idea of (7) and the performance depends on the selection of the M-estimator influence function $\psi(\cdot)$. In our cases, the rate of descent for Cauchy M-estimator (9) is:

$$\psi(e_k) \triangleq \frac{e_k}{1 + e_k^2}, \quad w(e_k) \triangleq \frac{1}{1 + e_k^2}. \quad (13)$$

After the convergence of Gauss-Newton iteration, the updated weights truly reflect the contribution of each acquired point. The points with small weights are outliers and needed to be eliminated. Then repeat IRLS optimisation process with the inliers. This robust registration approach is summarized in Algorithm 1.

IV. EXPERIMENTS AND RESULTS

A. Experimental datasets

Bone structure datasets. In this study, we selected several bone surface data from publicly available datasets that are all created from CT scans. [27]–[29]. RWTHmediTEC [27] only obtains femur and hip structures. VSDFull [28] includes the entire lower body which is a complementary version of RWTHmediTEC, and SSM-Tibia [29] only has the right tibia.

TABLE I
SUMMARY OF THE BONE STRUCTURE DATASETS. L AND R IN TABLE STAND FOR LEFT AND RIGHT, RESPECTIVELY.

Dataset	Femur		Hip		Tibia	
	R	L	R	L	R	L
RWTHmediTEC [27]	19	18	20	20	-	-
VSDFull [28]	30	30	30	30	30	30
SSM-Tibia [29]	-	-	-	-	30	-

The detailed composition of the dataset is reported in Table I. For example, RWTHmediTEC contains 19 right and 18 left femurs, and 20 each of the left and right hip structures.

Partial point sets generation. The partial point sets were generated from the models, and shaped as curved to simulate the acquired points by moving the surgical probe (refer to the yellow dots in Fig. 3). The points were distributed only on the proximal femur and acetabulum exposed in THR, and on the proximal tibia, medical and lateral femoral condyle exposed in TKA (Fig. 3). We applied a rigid random transformation to the partial point sets, involving a rotation R on each axis within -45 to 45 degrees in each of three axes, and a translation t within -1000 mm to 1000 mm for each element to serve as the ground truth.

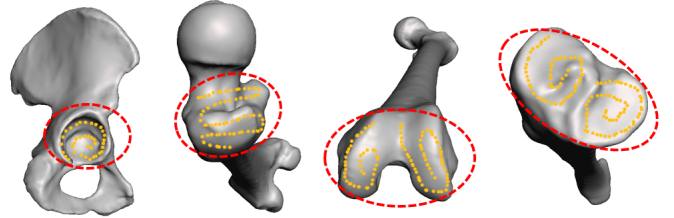


Fig. 3. The parts circled in red dotted lines are bone structures that may be exposed during orthopaedic surgeries. In order from left to right: pelvic acetabulum; proximal femur; femoral condyle; proximal tibia. The yellow points are the simulated surgical probe picking points, which are used as partial data to be registered with the full point cloud model.

B. Comparison with benchmarks

In this study, we compared our proposed method with several benchmarks including ICP [4], CPD [8], JRMPC [32], and Go-ICP [31]. Optical tracking and electromagnetic tracking are the most commonly used intra-operative medical devices to acquire partial point set. The accuracy (root mean square error) of optical tracking and electromagnetic tracking are 0.15 mm and 0.7 mm, respectively [37]. Therefore, the zero-mean Gaussian noises were injected into the acquired partial point sets (refer to Fig. 3) to simulate the noise interference during acquisition. In terms of *isotropic* positional noise, the standard deviation is $[0.5, 0.5, 0.5]$ mm, while $[0.3, 0.5, 0.7]$ mm under *anisotropic* positional noise. The quantitative metrics we used to evaluate the effectiveness of the proposed registration method were mean absolute errors (MAE) over Euler angles of R and translation vector t , as well as Chamfer Distance (CD) which is the average distance between each point in one set to its nearest neighbor found in another [30].

Table II shows the comparison results by using different methods for various bone structures. The best results are

TABLE II
REGISTRATION RESULTS ON VARIOUS BONE DATASETS USING DIFFERENT METHODS

Noise Type	Methods	Hip			Proximal Femur			Femoral Condyle			Proximal Tibia		
		MAE (R/deg)	MAE (t/mm)	CD (mm)	MAE (R/deg)	MAE (t/mm)	CD (mm)	MAE (R/deg)	MAE (t/mm)	CD (mm)	MAE (R/deg)	MAE (t/mm)	CD (mm)
Isotropic	ICP	42.102	4.672	5.208	21.865	93.490	4.344	47.69	99.024	9.077	64.320	80.729	4.986
	CPD	21.327	9.855	6.384	30.553	95.697	4.414	59.811	108.143	8.070	60.485	72.098	4.855
	JRMPC	18.932	3.321	3.231	22.735	80.523	4.163	21.638	91.427	8.142	41.648	73.831	4.073
	Go-ICP	2.131	0.269	0.765	2.837	2.024	1.008	1.242	0.948	1.071	1.125	1.564	0.804
	Proposed	0.204	0.202	0.706	0.518	0.667	0.846	0.605	0.473	0.904	1.127	0.763	0.736
Anisotropic	ICP	43.743	17.868	5.289	22.358	92.215	4.398	49.496	98.201	9.013	65.151	79.499	4.789
	CPD	21.853	29.376	6.349	31.701	96.082	4.567	59.695	109.572	8.186	59.957	72.367	4.976
	JRMPC	19.343	23.275	3.458	23.748	80.145	4.124	23.953	96.341	9.742	40.273	73.164	4.267
	Go-ICP	3.718	0.403	0.807	3.154	3.037	1.005	1.780	0.431	0.979	6.153	2.857	0.846
	Proposed	0.752	0.177	0.691	0.731	0.557	0.889	0.63	0.408	0.952	1.304	0.945	0.811

bolded. Due to the excessive distribution disparity between the full and partial point sets, ICP, CPD and JRMPC performed poorly. Especially for slender bones such as the femur and tibia, these methods can easily fall into a local minima where the intra-operative sparse points converge to the middle of the femoral or tibial shaft, even given a good initial guess. Go-ICP performed much better when the mean squared error (MSE) convergence threshold is set to a very small value ($1e-5$). Our approach can always achieve the lowest MAE over Euler angles and translation vector in most test cases. We also try to get results from TEASER [5]. Unfortunately, TEASER is not able to handle two point clouds that are disparate in number and have a tiny fraction of overlap.

C. Resilience to noise and outliers

In orthopedic surgery, the intra-operatively acquired points are usually disturbed by noise and the low-quality point sets may affect the accuracy of the registration. Therefore, it is necessary to verify the robustness of the proposed method in the presence of noise. We injected different levels of Gaussian noise into the acquired point set. The *isotropic* positional noise levels increased gradually from 0.5 mm to 1.2 mm. The standard deviation of *anisotropic* positional noise increased gradually from [0.3, 0.5, 0.7] mm to [1.0, 1.2, 1.4] mm. The registration results in Table III are integrated for datasets of various bone types and demonstrate the resilience of our method in the face of noise disruptions. The proposed method performs well and converges fast under reasonable noise.

TABLE III
REGISTRATION RESULTS ON DIFFERENT NOISE LEVEL

Noise Type	Noise Levels (mm)	MAE (R/deg)	MAE (t/mm)	CD (mm)	Time (s)
Isotropic	0.5	0.614	0.526	0.798	0.077
	0.7	0.670	0.782	0.836	0.151
	0.9	1.021	0.976	1.057	0.441
	1.2	1.168	1.029	1.201	0.653
Anisotropic	[0.3,0.5,0.7]	0.854	0.522	0.836	0.313
	[0.5,0.7,0.9]	0.674	0.797	0.895	0.774
	[0.7,0.9,1.1]	1.077	0.676	1.054	0.59
	[1.0,1.2,1.4]	1.575	0.944	1.169	0.674

The intra-operative acquired partial points may also be susceptible to outliers due to interference between med-

ical devices. To address this issue, we validated our proposed method by injecting various ratios of outliers {10%, 30%, 50%, 70%, 90%} into the partial point sets. The injected outliers were randomly distributed around the bone model and the ratios are calculated as $N_{out}/(N_{in} + N_{out})$. The positional noise injected is the same as Section IV-B. As shown in Table IV, the proposed method is robust to increasing injected outliers up to 90%. As it is highlighted in bold, the largest rotational and translation error values are around 1.1 degree and 0.7 mm, which is still acceptable for a typical orthopedic surgery. The proposed method also performed well in terms of convergence speed, taking no more than 0.5 seconds except for the extreme case of 90% outliers.

D. Real phantom experiments

The proposed method was also tested in phantom experiments (Fig. 4). Both optical tracking system (OTS) and electromagnetic tracking (EMT) setups were used. The OTS we used is the Polaris Vega XT (Northern Digital Inc., Canada) and the EMT is the Aurora® electromagnetic tracking (Northern Digital Inc., Canada) with tabletop field generator. The phantom experiments were performed using four hip and three femur sawbones models under each of the two tracking systems. The sawbones models were scanned in advanced by a structured light 3D scanner Solutionix C500, and the respective gradient-SDFs were generated.

During the experiments, the acquisition frequencies of OTS and EMT were 80 Hz and 40 Hz, respectively. The number

TABLE IV
REGISTRATION RESULTS ON DIFFERENT OUTLIER RATES

Noise Type	Outlier Ratio	MAE (R/deg)	MAE (t/mm)	CD (mm)	Time (s)
Isotropic	10%	0.574	0.456	0.786	0.109
	30%	0.682	0.456	0.806	0.069
	50%	0.615	0.487	0.803	0.281
	70%	0.682	0.481	0.853	0.288
	90%	0.961	0.608	0.903	2.320
Anisotropic	10%	0.732	0.475	0.835	0.081
	30%	0.724	0.471	0.835	0.106
	50%	0.796	0.489	0.846	0.134
	70%	0.899	0.478	0.875	0.482
	90%	1.104	0.691	0.852	2.714

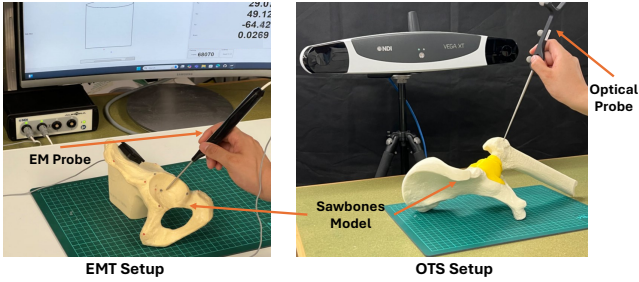


Fig. 4. Setups: repeated trials were performed with the sawbones models in each of the two tracking systems. Points were collected by moving the probe over the pelvic acetabulum and proximal femur.

of points taken in the pelvic acetabulum and proximal femur by the surgical probe were 600 and 1000, respectively (Fig. 5). Since there is no ground truth, we use target registration error (TRE) to quantify the registration accuracy of our method. We selected 10 anatomical landmarks as targets for the **entire bone model**, in stead of the small selection in pelvic acetabulum or proximal femur. Suppose anatomical landmarks on the pre-model are defined as P_{tar}^{pre} . In the experiments, these landmarks are also simultaneously need to be recognised on the sawbones model and acquired by the probe, and are denoted as P_{tar}^{intra} . Then the TRE can be calculated as:

$$TRE = \|\hat{R} \cdot P_{tar}^{intra} + \hat{t} - P_{tar}^{pre}\|, \quad (14)$$

where \hat{R} and \hat{t} are the registration result. It is worth noting that these anatomical landmarks were not involved in the registration calculation. As shown in Table V, the proposed framework can achieve TRE value of 2.198 mm and 2.719 mm in optical and electromagnetic tracking systems, respectively, which is much more accurate than the other methods.

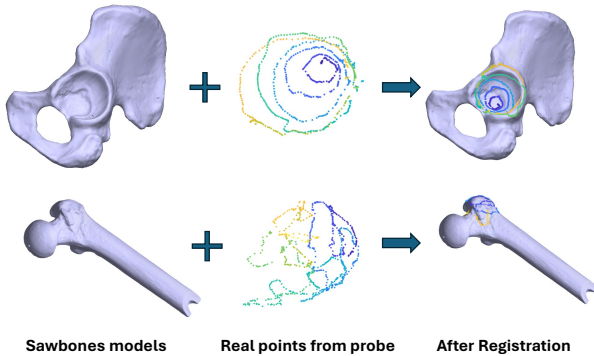


Fig. 5. Two examples of the real data from phantom experiments.

V. DISCUSSION

In computer-assisted orthopedic surgery, the registration of partial-to-full bone point sets presents several challenges, including partially overlapped and noise interference. We propose a novel and effective registration framework based on gradient-SDF to address these challenges.

Why gradient-SDF. Gradient-SDF can pre-calculate and store the closest distance from each spatial location to the

TABLE V
REGISTRATION RESULTS IN PHANTOM EXPERIMENTS

Tracking System	Methods	Hip		Femur	
		TRE (mm)	CD (mm)	TRE (mm)	CD (mm)
Optical	ICP	102.970	3.515	182.340	3.641
	CPD	92.212	4.705	30.426	3.962
	JRMPC	51.342	3.327	35.540	4.013
	Go-ICP	6.782	0.665	4.563	0.721
	Proposed	2.198	0.505	2.316	0.636
Electromagnetic	ICP	109.851	4.264	120.457	4.396
	CPD	87.237	4.297	34.225	3.846
	JRMPC	57.325	3.452	37.406	3.261
	Go-ICP	7.314	0.691	4.713	1.103
	Proposed	2.719	0.662	3.174	1.240

surface of geometry, and the intra-operative acquisition points in COAS only occur on the surface of bone, so it is appropriate to represent the bone model as gradient-SDF for registration. Moreover, gradient-SDF naturally contains the geometric properties that are not present in the gradients calculated by standard SDF [23]. So the convergence is better and faster for sparse point set without the need for correspondences.

Initial guess. Although the proposed framework is a correspondence-free registration method, it still requires to provide an initial guess. During our experiments, we found that our method is quite robust to inaccurate initial translation, but does require a reasonable initial rotation. In practice, a good initial rotation can be obtained by asking the surgeon to point to 3 anatomical landmarks. Compared with more than 30 points required by MAKO robot, getting a better initial value with 3 points does not add much time cost and can be easily accepted by the surgeons.

Limitation. From the clinical application point of view, it would be desirable to include metrics in the current framework that allow real-time assessment of whether the surgeon has acquired enough intra-operative points. We also plan to integrate our proposed framework into the surgical robotic system [39], [40] and perform cadaver experiments in the future.

VI. CONCLUSION

This paper presents a novel and effective registration framework based on gradient-SDF to address the challenges of partial-to-full bone registration in computer-assisted orthopedic surgery. Experiments on multi-category bone structures demonstrate that our proposed framework can provide more accurate results than the state-of-the-art registration methods and be robust to 90% outliers. The gradient-SDF results in the accurate and fast convergence for sparse and partially overlapped point set without the need for correspondences. Our method can achieve convergence in less than 1 second in real scenarios and mean target registration error values as low as 2.198 mm for the entire bone model. The proposed framework enables registration to be accomplished by merely guiding the probe over the bone surface to acquire random points, thus simplifies the surgeon's intra-operative workflow and shows great potential clinical value.

REFERENCES

- [1] N. Sugano, "Computer-assisted orthopedic surgery," *Journal of Orthopaedic Science*, vol. 8, pp. 442–448, 2003.
- [2] B. Ma and R. E. Ellis, "Robust registration for computer-integrated orthopedic surgery: laboratory validation and clinical experience," *Medical image analysis*, vol. 7, no. 3, pp. 237–250, 2003.
- [3] Z. Min, A. Zhang, Z. Zhang, J. Wang, S. Song, H. Ren, and M. Q.-H. Meng, "3d rigid point set registration for computer-assisted orthopedic surgery (caos): A review from the algorithmic perspective," *IEEE Transactions on Medical Robotics and Bionics*, 2023.
- [4] P. J. Besl and N. D. McKay, "Method for registration of 3-d shapes," in *Sensor fusion IV: control paradigms and data structures*, vol. 1611. Spie, 1992, pp. 586–606.
- [5] H. Yang, J. Shi, and L. Carlone, "Teaser: Fast and certifiable point cloud registration," *IEEE Transactions on Robotics*, vol. 37, no. 2, pp. 314–333, 2020.
- [6] J. Serafin and G. Grisetti, "Nip: Dense normal based point cloud registration," in *2015 IEEE/RSJ International Conference on Intelligent Robots and Systems (IROS)*. IEEE, 2015, pp. 742–749.
- [7] B. Jian and B. C. Vemuri, "Robust point set registration using gaussian mixture models," *IEEE transactions on pattern analysis and machine intelligence*, vol. 33, no. 8, pp. 1633–1645, 2010.
- [8] A. Myronenko and X. Song, "Point set registration: Coherent point drift," *IEEE transactions on pattern analysis and machine intelligence*, vol. 32, no. 12, pp. 2262–2275, 2010.
- [9] G. D. Evangelidis, D. Kounades-Bastian, R. Horaud, and E. Z. Psarakis, "A generative model for the joint registration of multiple point sets," in *European Conference on Computer Vision*. Springer, 2014, pp. 109–122.
- [10] C. R. Qi, H. Su, K. Mo, and L. J. Guibas, "Pointnet: Deep learning on point sets for 3d classification and segmentation," in *Proceedings of the IEEE conference on computer vision and pattern recognition*, 2017, pp. 652–660.
- [11] Y. Wang, Y. Sun, Z. Liu, S. E. Sarma, M. M. Bronstein, and J. M. Solomon, "Dynamic graph cnn for learning on point clouds," *ACM Transactions on Graphics (tog)*, vol. 38, no. 5, pp. 1–12, 2019.
- [12] Y. Aoki, H. Goforth, R. A. Srivatsan, and S. Lucey, "Pointnetlk: Robust & efficient point cloud registration using pointnet," in *Proceedings of the IEEE/CVF conference on computer vision and pattern recognition*, 2019, pp. 7163–7172.
- [13] Y. Wang and J. M. Solomon, "Prnet: Self-supervised learning for partial-to-partial registration," *Advances in neural information processing systems*, vol. 32, 2019.
- [14] Y. Wang and J. Solomon, "Deep closest point: Learning representations for point cloud registration," in *Proceedings of the IEEE/CVF international conference on computer vision*, 2019, pp. 3523–3532.
- [15] F. Chen, Q. Du, J. Zhao, Z. Zhao, D. Zhang, and H. Liao, "A generalized full-to-partial registration framework of 3d point sets for computer-aided orthopedic surgery," *IEEE Transactions on Biomedical Engineering*, 2023.
- [16] H. Ren and P. Kazanzides, "Investigation of attitude tracking using an integrated inertial and magnetic navigation system for hand-held surgical instruments," *IEEE/ASME Transactions on Mechatronics*, vol. 17, no. 2, pp. 210–217, 2010.
- [17] J. Wang, S. Song, H. Ren, C. M. Lim, and M. Q.-H. Meng, "Surgical instrument tracking by multiple monocular modules and a sensor fusion approach," *IEEE Transactions on Automation Science and Engineering*, vol. 16, no. 2, pp. 629–639, 2018.
- [18] T. Li, Y. Song, P. Walker, K. Pan, V. A. van de Graaf, L. Zhao, and S. Huang, "A closed-form solution to electromagnetic sensor based intraoperative limb length measurement in total hip arthroplasty," in *International Conference on Medical Image Computing and Computer-Assisted Intervention*. Springer, 2023, pp. 365–375.
- [19] S. Zhang, L. Zhao, S. Huang, H. Wang, Q. Luo, and Q. Hao, "Slam-tka: Real-time intra-operative measurement of tibial resection plane in conventional total knee arthroplasty," in *International Conference on Medical Image Computing and Computer-Assisted Intervention*. Springer, 2022, pp. 126–135.
- [20] V. Gopalakrishnan, N. Dey, and P. Golland, "Intraoperative 2d/3d image registration via differentiable x-ray rendering," in *Proceedings of the IEEE/CVF Conference on Computer Vision and Pattern Recognition*, 2024, pp. 11 662–11 672.
- [21] Z. Min, D. Zhu, and M. Q.-H. Meng, "Robust and accurate 3d curve to surface registration with tangent and normal vectors," in *2020 IEEE International Conference on Robotics and Automation (ICRA)*. IEEE, 2020, pp. 9953–9959.
- [22] J. H. Lonner, *Robotics in knee and hip arthroplasty: current concepts, techniques and emerging uses*. Springer, 2019.
- [23] C. Sommer, L. Sang, D. Schubert, and D. Cremers, "Gradient-sdf: A semi-implicit surface representation for 3d reconstruction," in *Proceedings of the IEEE/CVF Conference on Computer Vision and Pattern Recognition*, 2022, pp. 6280–6289.
- [24] G. Hu, K. Khosoussi, and S. Huang, "Towards a reliable slam back-end," in *2013 IEEE/RSJ International Conference on Intelligent Robots and Systems*. IEEE, 2013, pp. 37–43.
- [25] A. Blake and A. Zisserman, *Visual reconstruction*. MIT press, 1987.
- [26] Z. Zhang, "Parameter estimation techniques: A tutorial with application to conic fitting," *Image and vision Computing*, vol. 15, no. 1, pp. 59–76, 1997.
- [27] M. C. Fischer, S. A. Grothues, J. Habor, M. de la Fuente, and K. Radermacher, "A robust method for automatic identification of femoral landmarks, axes, planes and bone coordinate systems using surface models," *Scientific Reports*, vol. 10, no. 1, p. 20859, 2020.
- [28] M. C. Fischer, "Database of segmentations and surface models of bones of the entire lower body created from cadaver ct scans," *Scientific Data*, vol. 10, no. 1, p. 763, 2023.
- [29] M. Keast, J. Bonacci, and A. Fox, "Geometric variation of the human tibia-fibula: a public dataset of tibia-fibula surface meshes and statistical shape model," *PeerJ*, vol. 11, p. e14708, 2023.
- [30] F. Lin, Y. Yue, S. Hou, X. Yu, Y. Xu, K. D. Yamada, and Z. Zhang, "Hyperbolic chamfer distance for point cloud completion," in *Proceedings of the IEEE/CVF international conference on computer vision*, 2023, pp. 14 595–14 606.
- [31] J. Yang, H. Li, D. Campbell, and Y. Jia, "Go-icp: A globally optimal solution to 3d icp point-set registration," *IEEE transactions on pattern analysis and machine intelligence*, vol. 38, no. 11, pp. 2241–2254, 2015.
- [32] G. D. Evangelidis and R. Horaud, "Joint alignment of multiple point sets with batch and incremental expectation-maximization," *IEEE transactions on pattern analysis and machine intelligence*, vol. 40, no. 6, pp. 1397–1410, 2017.
- [33] A. Segal, D. Haehnel, and S. Thrun, "Generalized-icp," in *Robotics: science and systems*, vol. 2, no. 4. Seattle, WA, 2009, p. 435.
- [34] S. D. Billings, E. M. Boctor, and R. H. Taylor, "Iterative most-likely point registration (impl): A robust algorithm for computing optimal shape alignment," *PloS one*, vol. 10, no. 3, p. e0117688, 2015.
- [35] R. H. Taylor, P. Kazanzides, G. S. Fischer, and N. Simaan, "Medical robotics and computer-integrated interventional medicine," in *Biomedical Information Technology*. Elsevier, 2020, pp. 617–672.
- [36] R. Arun Srivatsan, N. Zavallos, P. Vagdari, and H. Choset, "Registration with a small number of sparse measurements," *The International Journal of Robotics Research*, vol. 38, no. 12-13, pp. 1403–1419, 2019.
- [37] A. Sorrento, M. B. Porfido, S. Mazzoleni, G. Calvosa, M. Tenucci, G. Ciuti, and P. Dario, "Optical and electromagnetic tracking systems for biomedical applications: A critical review on potentialities and limitations," *IEEE reviews in biomedical engineering*, vol. 13, pp. 212–232, 2019.
- [38] P. Babin, P. Giguere, and F. Pomerleau, "Analysis of robust functions for registration algorithms," in *2019 International Conference on Robotics and Automation (ICRA)*. IEEE, 2019, pp. 1451–1457.
- [39] P. Walker, T. Li, R. Khonasty, K. Ponnanna, A. Kuo, L. Zhao, and S. Huang, "Proof of concept study for using ur10 robot to help total hip replacement," *The International Journal of Medical Robotics and Computer Assisted Surgery*, vol. 18, no. 2, p. e2359, 2022.
- [40] T. Li, P. Walker, R. Khonasty, V. A. van de Graaf, E. Yelf, L. Zhao, and S. Huang, "Robotic-assisted burring in total hip replacement: A new surgical technique to optimise acetabular preparation," *The International Journal of Medical Robotics and Computer Assisted Surgery*, vol. 20, no. 1, p. e2615, 2024.